

Enhanced microwave performance of cobalt nanoflakes with strong shape anisotropy

Fei Ma,¹ Yong Qin,^{1,a)} and Yun-Ze Li²

¹*Institute of Nanoscience and Nanotechnology, Lanzhou University, Lanzhou 730000, People's Republic of China*

²*School of Aeronautic Science and Engineering, Beihang University, Beijing 100191, People's Republic of China*

(Received 7 April 2010; accepted 1 May 2010; published online 19 May 2010)

Co nanoflakes are synthesized through a low temperature hydrothermal method. The single-phased hexagonal close-packed Co nanoflakes have a diameter of several micrometers and a thickness about 80 nm. Magnetic hysteresis loops are quite different along different directions deviating from the nanoflakes plane, which shows Co nanoflakes have strong magnetic anisotropy. Flakelike morphology influence the performance of complex permeability in gigahertz frequency. Natural resonance peak happens at 5.74 GHz with the contribution of shape anisotropy. Multiple resonance phenomenon appears due to the exchange resonance effect, which makes Co nanoflakes a broadband candidate for microwave absorbing material. © 2010 American Institute of Physics. [doi:10.1063/1.3432441]

In order to extend the application of ferromagnetic materials in high density recording media, magnetic field sensor, electromagnetic wave absorption, and, etc., considerable research has focused on magnetic particles in nanometer scale.^{1,2} For those small structures, interesting changes of magnetic behavior are expected, as the particle size becomes comparable to the physical characteristic lengths such as the exchange length or the domain wall width.³ The well defined shapes make it possible to control the demagnetizing field, the domain structure and, in some cases, the microwave properties including high frequency permeability and resonance behaviors. Theoretical analysis and experimental investigations on the submicron-sized anisotropic particles indicate that control of the morphology of the ferromagnetic particles is needed since the gyromagnetic resonance is highly dependent on the particle shape through the effect of the demagnetizing field.⁴⁻⁶ The anisotropic particles may have a higher resonance frequency and exceed the Snoek's limit in the gigahertz frequency range owing to their large shape anisotropy, making these material such as Co nanoflakes the ideal material for electromagnetic wave absorption in relatively high frequency range.

Co nanoflakes were synthesized by a low temperature hydrothermal method. 20 ml 0.1 mol/L CoCl₂, 2 ml 0.1 mol/L hexadecyl trimethyl ammonium bromide (CTAB), 0.8 ml 25 mol/L NaOH and 2 ml 85% aqueous hydrazine were mixed together under magnetic stirring. The feedstock was transferred into a 100 ml teflon-lined autoclave. Hydrothermal synthesis was performed at 180 °C for 1h. After washing and drying, the powders were collected. Co nanoflakes-paraffin wax composite sample was prepared by uniformly mixing Co and paraffin matrix and compacted into ring shape of 7.00 mm outer diameter and 3.04 mm inner diameter for microwave property measurements. Figures were taken on a Hitachi S-4800 scanning electron microscope (SEM) and Hitachi H-600 transmission electron microscopy (TEM). The crystal structure was characterized by x-ray dif-

fraction (XRD) with Cu K α radiation. Magnetic and microwave properties were studied using a Lake Shore 7304 vibrating sample magnetometer and an APC7 coaxial line mode with an Agilent PNA E8363B network analyzer at room temperature.

Figure 1(a) shows the Co powder is composed of nanoflakes with sizes of several micrometers. The lateral view of a nanoflake shown in Fig. 1(b) illuminates the thickness about 80 nm. The inset of Figure 1(c) shows the selected area electron diffraction pattern exhibiting sixfold symmetry with the electron beam being along the $\langle 001 \rangle$ zone axis of the hexagonal close-packed (hcp) crystal structure, implying that the nanoflakes are single crystals and the growth of (001) plane was inhibited during the process of crystal growth. CTAB, a common used anionic surfactant in

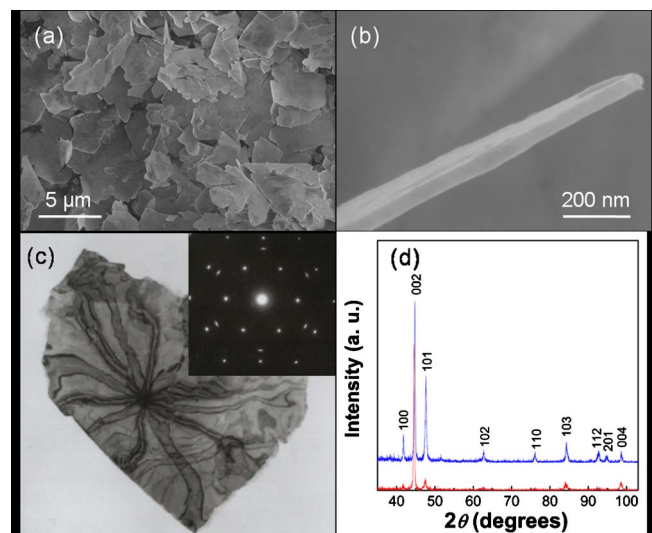


FIG. 1. (Color online) The SEM micrographs of Co nanoflakes (a), and the lateral view of a nanoflake (b); Bright field TEM image, the inserted image is the electron diffraction pattern (c); The XRD patterns of the Co nanoflakes powders (upper) and the disk compacted with Co nanoflakes (lower).

^{a)}Electronic mail: yqin@lzu.edu.cn.

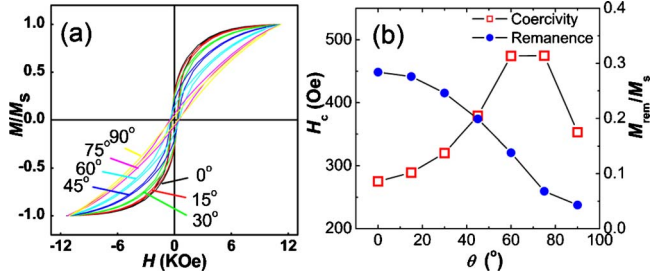


FIG. 2. (Color online) Magnetic hysteresis loops of the disk compacted from Co nanoflakes with different deviating angles between the applied magnetic field and the in-plane direction (a); Coercivity and remanence as a function of the angles between the applied magnetic field and the in-plane direction of Co nanoflakes (b).

morphology control, serves as capping reagent which might preferentially absorb on (001) plane in crystal growth resulting in the flake-like morphology.⁷ XRD data of the upper one in Fig. 1(d) confirms the hcp phase of Co nanoflakes. The lower one is the XRD data of the sample by compacting nanoflakes into a disk with diameter of 6 mm and the thickness about 0.26 mm in a mold. The nanoflakes tend to align in a parallel direction with each other and parallel with the surface plane of the compacted disk under pressure. The relative intensity of (002) peak increase drastically, indicating the compacted disks have strong hcp [001] preferred orientations.

Figure 2(a) shows the measured magnetic hysteresis loops of the disk compacted from Co nanoflakes along the directions deviating different angle θ from the in-plane direction. It can be seen that the easy magnetization axis is in-plane direction. The switching field increases with the angle θ , reaches its maximum at about 60°, and then decreases. From Fig. 2(b), we can see that the variation of the coercivities with the angle θ consists with that of switching field. At the same time, it can be seen that the remanence decreases with the angle θ monotonously. For a nanoflake, the in-plane demagnetization field is much smaller than the demagnetization field out of the plane, making the magnetic moments easier to align in in-plane direction.

The microwave properties of Co nanoflake-paraffin wax composites with 10.0 vol % of Co was investigated in the range of 0.1–15 GHz. Figure 3(a) shows that the real part ϵ' and imaginary part ϵ'' of the complex permittivity maintained almost a constant over 0.1–15 GHz except for the little fluctuation above 12 GHz. In the metal-insulator composites, the space charge and the dipole polarization could be ascribed to the polarization phenomena.⁸ With the frequency increases, the dipolar polarization dominated in the metal-insulator composites, resulting in the fluctuation of complex permittivity above 12 GHz. Figure 3(b) shows that the μ' values decrease with frequency, while μ'' values show three broad resonance peaks around 5.74, 7.79, and 12.00 GHz in the 0.1–15 GHz frequency range. To further understand the multiple resonance behavior, the spectrum was fitted as the linear overlap of three resonance peaks P₁, P₂, and P₃. The μ' and μ'' were calculated by fitting the Landau–Lifshitz–Gibert equations,⁹

$$\mu' = B + \sum_{i=1}^3 I_i \frac{[1 - (f/f_i)^2(1 - \alpha_i^2)]}{[1 - (f/f_i)^2(1 + \alpha_i^2)]^2 + 4\alpha_i^2(f/f_i)^2}, \quad (1)$$

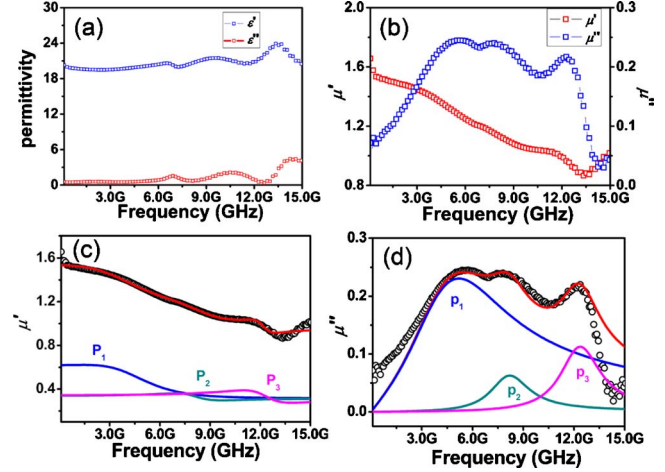


FIG. 3. (Color online) Frequency dependence of the complex permittivity (a) and permeability (b), and the fitting curves of the real part (c) and imaginary part (d) of permeability.

$$\mu'' = \sum_{i=1}^3 I_i \frac{(f/f_i)\alpha_i[1 + (f/f_i)^2(1 + \alpha_i^2)]}{[1 - (f/f_i)^2(1 + \alpha_i^2)]^2 + 4\alpha_i^2(f/f_i)^2}, \quad (2)$$

where f is frequency, f_i is the spin resonance frequency, α_i is the damping coefficient, and I_i is the intensity of the peak. First, the triple resonance peaks of the μ'' curve was fitted. Then, the μ' curve was calculated using the obtained fitting parameters. Figures 3(c) and 3(d) show the fitted real part and imaginary part of the permeability with the fitting parameters listed in Table I.

The first resonance peak around 6.86 GHz can be ascribed to natural resonance. The resonance frequencies vary linearly with the effective anisotropic field which is found to depend on the crystalline anisotropy, magnetic particle geometry, particle size, and interaction of magnetic particles. As discussed above, when the geometry of nanoparticle becomes flake-like, its magnetization will be in the plane of the flake and the reversal and oscillation of magnetization will be restricted in the flake plane too. According to the natural resonance equation, the resonance frequency for an ellipsoid is given by the Kittel equation,⁴

$$f_r = \frac{\gamma}{2\pi} \{ [H_i + (N_y - N_z)M_s] \times [H_i + (N_x - N_z)M_s] \}^{1/2}, \quad (3)$$

where M_s is the saturation magnetization (1.4×10^6 A/m for hcp Co), N_x , N_y , and N_z are the demagnetizing factors along the x , y , and z axes of the coordinate system, supposed that x -axis being out of plane, and y -axis and z -axis being in-plane. For Co nanoflakes with diameter about 4 μm and thickness about 80 nm, the calculated demagnetizing factors

TABLE I. Fitting parameters for permeability dispersion spectra. $f(\text{max})$ and $f(\text{fit})$ are the experimental and fitted resonance frequency. I is the intensity of the peak and α is the damping coefficient.

	$f(\text{max})$ (GHz)	$f(\text{fit})$ (GHz)	I	α
Natural resonance (P1)	5.74	6.86	0.30	0.81
Exchange resonance (P2)	7.79	8.32	0.021	0.17
Exchange resonance (P3)	12.00	12.45	0.026	0.12

are $N_x=0.970$ and $N_y=N_z=0.015$.¹⁰ H_i is the in-plane anisotropic field along z axis. The in-plane anisotropy might be introduced from the irregular in-plane morphology of nanoflakes and the magnetic exchange interaction. However, the in-plane anisotropic field is difficult to be calculated, since magnetocrystalline anisotropy, shape anisotropy, and magnetic interaction all contribute to the in-plane anisotropic field. Deng *et al.* suggested using the coercive force H_c to replace the effective anisotropic field.¹¹ For our case, we also expect that the in-plane anisotropic field H_i is around the in-plane coercivity. Based on the parameters mentioned above, the natural resonance frequency f_r is equal to 6.04 GHz, which matches satisfactorily with our fitted frequency for natural resonance.

The resonance peaks around 8.32 and 12.45 GHz should be ascribed to exchange resonance. Multiple resonance is a subject of controversy in nanoparticles. Among those modes which deal with multiple resonance, the most accepted one is the exchange resonance mode proposed by Aharoni.¹² In our case, due to the nanoscaled size of Co nanoflakes, surface anisotropy and exchange energy caused by exchange effect would be evidenced. According to the exchange resonance mode, the resonance frequencies are calculated by $\omega/\gamma = 2A\mu_{kn}^2/R^2M_s + H_s$, where A is the exchange constant, μ_{kn} are the roots of the differential spherical Bessel functions,¹² γ is the gyromagnetic ratio, R is the particle size, and H_s is the magnetostatic field. From the equation above, the exchange resonance frequencies are related to the squares of μ_{kn} . So, it is reasonable that the resonance peaks appear in higher frequency range due to the exchange effect for our Co nanoflake sample. Moreover, it is believed that the coexistence of natural resonance and exchange resonance is benefi-

cial to large bandwidth as a microwave absorber.

In conclusion, hcp Co nanoflakes are synthesized through the low temperature hydrothermal method. Coercivities and remanences are dominated by the shape anisotropy of nanoflakes due to the influence of demagnetization energy. A triple resonance behavior depending on the geometry and mean particle size is detected. The geometry contributes to the natural resonance peak, and the exchange energy and size effect can be qualitatively related to exchange resonance mode.

This research was supported by NSFC, NCET, Ph.D. Programs Foundation of Ministry of Education of China.

¹N. Dao, S. R. Homer, and S. L. Whittenburg, *J. Appl. Phys.* **86**, 3262 (1999).

²X. F. Zhang, X. L. Dong, H. Huang, Y. Y. Liu, W. N. Wang, X. G. Zhu, B. Lv, J. P. Lei, and C. G. Lee, *Appl. Phys. Lett.* **89**, 053115 (2006).

³T. Aign, P. Meyer, and S. Lemerle, *Phys. Rev. Lett.* **81**, 5656 (1998).

⁴C. Kittel, *Phys. Rev.* **73**, 155 (1948).

⁵F. Ma, J. Huang, J. Li, and Q. Li, *J. Nanosci. Nanotechnol.* **9**, 3219 (2009).

⁶J. Liu, M. Itoh, M. Terada, T. Horikawa, and K. Machida, *Appl. Phys. Lett.* **91**, 093101 (2007).

⁷Y. Xia, P. Yang, Y. Sun, Y. Wu, B. Mayers, B. Gates, Y. Yin, F. Kim, and H. Yan, *Adv. Mater.* **15**, 353 (2003).

⁸B. Lu, X. L. Dong, H. Huang, X. F. Zhang, X. G. Zhu, J. P. Lei, and J. P. Sun, *J. Magn. Magn. Mater.* **320**, 1106 (2008).

⁹A. Aharoni, *Introduction to the Theory of Ferromagnetism* (Clarendon, Oxford, 1996), Chap. 8, p. 181.

¹⁰S. Chikazumi, *Physics of Ferromagnetism*, 2nd ed. (Oxford University Press, Oxford, 1997), p. 12.

¹¹L. J. Deng, P. H. Zhou, J. L. Xie, and L. Zhang, *J. Appl. Phys.* **101**, 103916 (2007).

¹²A. Aharoni, *J. Appl. Phys.* **69**, 7762 (1991).